Optimization of geometric and flow parameters of solar air heater roughened with artificial roughness by Taguchi method

MUKESH KUMAR SAHU[a*]
SHIVAM MISHRA[b]
AVINASH KUMAR[a]

[a] Cambridge Institute of Technology, Department of Mechanical Engineering, Tatisilwai, Ranchi, Jharkhand, Pin-835103, India

[b] G L Bajaj Institute of Technology and Management, Department of Mechanical Engineering, Greater Noida, Uttar Pradesh, Pin-201308, India

Abstract   The paper presents the investigation of the optimum design parameters of a solar air heater (SAH) having wire ribs as artificial roughness by using the Taguchi method. The solar air heater has arc shape roughness geometry with apex upstream flow on the absorber plate. The objective of this paper is to obtain a set of parameters that deliver maximum thermo-hydraulic performance. For this objective, a new parameter the thermo-hydraulic improvement parameter (η_{THIP}), has been introduced. For the present analysis, the effects of Reynolds number (Re), relative roughness pitch (P/e), angle of attack (α), and relative roughness height (e/D_h), denoted by A, B, C, and D, respectively, have been considered. An ($L_{18} = 6^1 \cdot 3^2$) orthogonal array (OA) was chosen as an experimental plan for applying the Taguchi method. The set of control factors for the solar air heater SAH which delivers the maximum Nusselt number (Nu), and minimum friction factor (fr) – are $A_6B_2C_2$, and $A_1B_1C_3$ respectively. To obtain the maximum THIP the experimental set-up requires only one single run using the parameter $A_6B_2C_2$, hence there is no need to run it all 54 times.

Keywords: Roughness; Nusselt number; Friction factor; Taguchi method; Optimization

---

*Corresponding Author. Email: mks.nitjsr@gmail.com

Nomenclature

A_c	–	surface area of the absorber plate, m^2
A_o	–	area of orifice plate, m^2
C_{pa}	–	specific heat of air, J/kgK
C_d	–	coefficient of discharge for orifice meter
D	–	hydraulic diameter of duct, m
e	–	roughness height, m
e/D_h	–	relative roughness height
f	–	friction factor
G	–	velocity of air, m/s
h	–	heat transfer coefficient, W/m^{2}K
H	–	depth or height of solar air heater duct, m
Δh	–	height of U-tube manometer fluid column, m
Δh_1	–	height of micromanometer fluid column, m
I	–	intensity of solar radiation, W/m^2
K_a	–	thermal conductivity of air, W/m K
L	–	length of solar air heater duct, m
$\dot{m}$	–	mass flow rate of air, kg/s
N	–	number of glass cover
Nu	–	Nusselt number
P	–	roughness pitch, m
P_m	–	pumping power, W
ΔP_D	–	pressure drop across the test section, N/m^2
ΔP_o	–	pressure drop across orifice meter, N/m^2
P/e	–	relative roughness pitch
Re	–	Reynolds number
Q_u	–	useful heat gain, W
SN-R	–	signal-to-noise ratio
T_a	–	ambient temperature, K
T_{bm}	–	mean temperature of the bottom plate, K
T_{fi}	–	air inlet temperature, K
T_{fm}	–	mean air temperature in the duct, K
T_{fo}	–	outlet air temperature, K
T_{pm}	–	mean absorber plate temperature, K
ΔT	–	rise in air temperature, K
W	–	width of solar air heater duct, m
W/H	–	aspect ratio of collector duct

Greek symbols

α	–	angle of attack, deg
β_R	–	ratio of orifice diameter (D_2) to pipe internal diameter (D_1)
ε	–	emissivity
η_{th}	–	thermal efficiency
η_{eff}	–	thermohydraulic (effective) efficiency
μ	–	absolute viscosity of air, Ns/m^2
ρ	–	air density, kg/m^3
ρ_m	–	density of fluid used in micromanometer, kg/m^3
ρ_u	–	density of fluid used in U-tube manometer, kg/m^3

Subscripts

c	–	glass cover
p	–	plate
r	–	roughened
s	–	smooth

Acronyms

DOE	–	design of experiment
GI	–	galvanized iron
OA	–	orthogonal array
SAH	–	solar air heater
THIP	–	thermo-hydraulic improvement parameter
THPP	–	thermo-hydraulic performance parameter

1   Introduction

Since energy demand is increasing globally and it will increase more rapidly in the coming years, we have to harness and obtain more energy from the various available non-conventional energy sources that are free, more reliable and environment-friendly.

Various studies on different types of solar air heaters (SAHs) and other solar thermal systems which are focused to convert solar energy into useful heat energy for various applications have been reported. Solar air heaters are the most used device in thermal energy conversion systems worldwide. Due to simplicity in construction and ease of operation SAHs are effectively used in various domestic, industrial, and agricultural applications such as drying crops, fruits and vegetables, room and space heating, preheating, dehydration of various products, and coal drying [1]. However, it has been found by investigators *via* their research that SAHs have low thermal efficiency (η_{th}) due to the poor thermal conductivity property of air and low heat exchange between the air and smooth absorber plate. In addition to these, irregular solar intensity and availability of solar energy throughout the day are also the other major reasons for the low thermal efficiency of the SAHs [2]. Hence, the different heat transfer augmentation techniques and modifications on SAH absorber plates are employed by the investigators to obtain enhanced heat transfer rates and thermal performances.

To improve the thermal performance of SAHs various enhancement techniques like the use of fins, baffles and obstacles have been adopted [3–5]. It further includes different types of absorber plates such as V-groove, corrugated type, application of packing bed and porous materials in the air-flow

path in the duct of SAH. Numerous research has also been carried out with the use of thin wire ribs as artificial roughness and its geometries on the absorber plate of the SAH to obtain higher efficiency and outlet air temperature (T_{fo}) compared to the smooth plate SAH. The presence of artificial roughness in the form of ribs breaks the laminar sublayer and it is responsible for creating turbulence in the path of core-fluid flow which increases the heat transfer rate [5].

It is reported by the researchers that the use of any type of heat transfer augmentation technique in SAHs enhances the heat transfer coefficient (h) but it also increases the friction factor (f) in terms of more pumping power (P_m) as compared to simple SAH. Therefore, in order to analyze the overall performance of a SAH, by using any type of heat transfer augmentation techniques, Webb and Eckert [6] and Lewis [7] proposed a thermo-hydraulic performance parameter (THPP) that evaluated the heat transfer and friction factor (pumping power) characteristics simultaneously of the enhanced SAH to the reference (smooth) SAH, which is discussed in details in the further section of the present paper. For optimizing different system and operating parameters like the number of glass covers (N), the emissivity of the absorber plate (ε_p), mean absorber plate temperature (T_{pm}), rise in the air temperature (ΔT), tilt angle (β), and solar radiation intensity (I) for smooth flat plate SAH, Varun *et al.* [8] have used stochastic iterative perturbation technique (SIPT).

Further, Rao and Waghmare [9] applied teaching learning based optimization (TLBO) to optimize the thermal efficiency of a flat plate SAH. Optimization of smooth absorber plate SAH has been done by Siddhartha *et al.* [10] by using the particle swarm optimization (PSO) algorithm. Chamoli [11] has used the preference selection index (PSI) approach for the optimization of a V-down perforated baffled roughened rectangular channel. Similarly, Chauhan *et al.* [12] have used the preference selection index (PSI) algorithm to optimize the thermal efficiency of impinging air jet SAH. Bilen *et al.* [13] employed the Taguchi method to optimize the heat transfer from the surface of a rectangular block. Varun *et al.* [14] performed their experimental work and used the Taguchi method to optimize the thermo-hydraulic (effective) efficiency of SAH duct roughened with combined inclined and transverse rib geometry. Aghaie *et al.* [15] performed CFD (computational fluid dynamics) simulation-based study to optimize the geometry of angled ribs SAH and its thermo-hydraulic efficiency by using the Taguchi method. An experimental study was performed by Chauhan *et al.* [16] who employed Taguchi design of experiments (DOE) method for optimizing the thermo-hydraulic performance parameter (THPP) of im-

pinging air jet SAH. Chamoli [17] applied the Taguchi method to optimize the flow and geometrical parameters of the roughened channel with V-down perforated baffles. Hu *et al.* [18] optimized the thermal efficiency of solar air collectors with holes on the baffle by the Taguchi method. The Taguchi method has also been used by investigators for the optimization of different types of heat exchangers [19, 20]. Kotcioglu *et al.* [21] used this method to optimize the plate-fins type heat exchanger. Similarly, Chamoli *et al.* [22] optimized the shape of the heat exchanger with compound inserts, whereas Zeng *et al.* [23] employed the Taguchi method for optimizing the heat exchanger with a vortex-generator fin.

The above literature review revealed that Taguchi optimization techniques have been used for the optimization of the thermo-hydraulic (effective) efficiency (η_{eff}), thermal efficiency and thermo-hydraulic performance parameter of the smooth plate, baffle, impinging air jets, and for roughened SAHs.

For calculation and analyzing the performance *via* experimental works, multiple runs or trials need to be carried out to analyze the effects of various roughness and flow parameters on the performance of the roughened SAHs. Also, investigating the effects of all roughness parameters on heat transfer, friction factor and thermo-hydraulic performance of SAHs is a very time-consuming process. The various types of equipment, different devices (to read the input and output data/parameters), and their cost are also involved in the fabrication of the experimental setup. By applying any of the optimization methods, we are able to predict and find the combination sets of design and flow parameters by which we will obtain the optimum (maximum) performance from the SAH, and this also allows to save time and cost.

In the last few years, the Taguchi method has been used widely as an optimization technique to optimize the performances of various devices which are used in heat transfer applications such as heat exchangers and various types of SAHs. It is the technique developed by Taguchi [24, 25] based on orthogonal arrays (OA) of experiments with optimum values of process parameters providing reduced variance. Taguchi method is one of the optimization techniques which has been extensively used to obtain the set/combination of system parameters to optimize the performance of the systems [26, 27]. It also helps to minimize the costs which are involved in running multiple experimental runs [28, 29].

Based on the above review, it can be seen that not many papers have been presented by the researchers, especially for the artificial roughened type SAHs to optimize its thermo-hydraulic performance parameter by using the Taguchi method (see Table 1).

Table 1: Summary of investigations carried out by researchers for different types of SAHs by using the Taguchi method.

Type of solar air heater	Orthogonal array	Parameters		Optimization factor	Authors and reference
		Definition	Range		
Transverse and inclined roughened solar air heater	L_{27} (3^3)	Relative roughness pitch (P/e)	3–8	Thermo-hydraulic (effective) efficiency (η_{eff})	Varun et al., 2009 [14]
		Mean plate temperature (T_{pm})	68–112		
		Irradiation (I)	800–1000		
		Reynolds number (Re)	1200–11600		
Impinging jet solar air heater	L_{16} (3^4)	Jet diameter ratio (D_j/D_j)	0.043–0.109	Thermo-hydraulic performance parameter (THPP)	Chauhan et al., 2017 [16]
		Streamwise pitch ratio (X/D_h)	0.435–1.739		
		Spanwise pitch ratio (X/D_h)	0.435–1.304		
Machined rib solar air heater	L_{16} (4^4)	Rib relative pitch (P/H)	1–2	Thermo-hydraulic performance parameter (THPP)	Aghaie et al., 2015 [15]
		Rib relative height (e/H)	0.05–0.75		
		Rib relative tip width (a/H)	0–1		
		Rib relative front projection ($s/(H-a)$)	0–1		
V-down perforated baffle rectangular channel	L_{16} (4^4)	Relative roughness pitch (P/e)	1–4	Nusselt number (Nu) and friction factor (f)	Chamoli, 2015 [17]
		Relative roughness height (e/D_h)	0.287–0.6		
		Open area ratio (β)	12–44		
		Reynolds number (Re)	4100–18600		
Holes on baffle solar air heater	L_{27} (4^3)	Hole size	1/2–1/6	Thermal efficiency (η_{th})	Hu et al., 2018 [18]
		Hole location	0–1/3		
		Hole number	3–9		
		Inlet flow rate (Re)	0.0044–0.0132		

A novel parameter, the thermo-hydraulic improvement parameter (η_{THIP}), which evaluates in equal proportions of the increment in Nusselt number and friction factor for the present enhanced roughened surface SAH compared to the conventional smooth plate surface SAH is introduced and applied as an optimization parameter.

In this paper, the extended work compared to what has been previously investigated by Sahu *et al.* [30,31] is presented. The objective is to determine the set and combination of flow and roughness parameters for experimental studies (for the present arc shape apex-upstream roughened SAH), that will provide and which delivers the maximum Nusselt number, thermo-hydraulic improvement parameter, and the minimum friction factor using the Taguchi-based design of experiment (DOE) method.

2   Details of the experimental set-up

The experimental set-up rig was designed and fabricated as per the guidelines of the American Society of Heating, Refrigerating and Air-Conditioning Engineers (ASHRAE) standards [32] and was installed at the terrace to conduct experiments in actual outdoor conditions. Figure 1 is the schematic representation of the detailed experimental setup. It consists of a centrifugal blower, two wooden rectangular ducts, galvanized iron (GI) pipes and GI sheets (for SAHs absorber and bottom plates), one main air control valve, orifice plates and flanges (for two ducts), U-tube manometers (for two ducts), micromanometers (for two ducts). Each rectangular duct is suitably divided into three subsections, i.e. entry, test, and exit sections with the length (L) of 650 mm, 1200 mm and 300 mm, respectively.
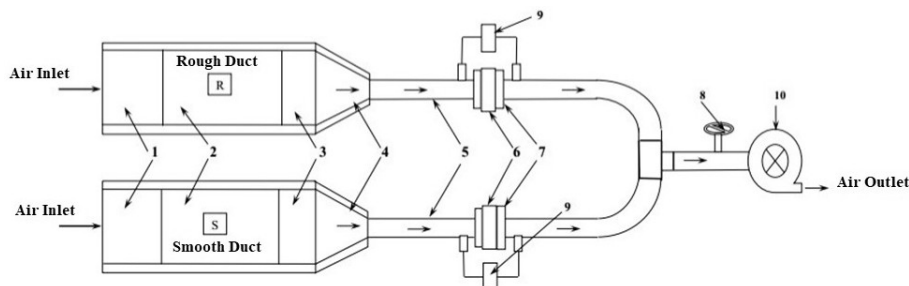

Figure 1: Schematic diagram of experimental set-up: 1 – entry section, 2 – test section, 3 – exit section, 4 – header, 5 – flow pipe, 6 – orifice meter, 7 – flange pipe, 8 – control valve, 9 – U-tube manometer, 10 – centrifugal suction blower.

The duct has a width of 330 mm (W) and 30 mm height (H) with an aspect ratio of $W/H = 11$.

One main air control valve (denoted by *8*) is used to regulate the mass flow rate of air in both SAH ducts. Two sides and the bottom of the duct were insulated with 50 mm thick glass wool insulation adequately. A glass of 4 mm thickness was used for glazing with a distance of 30 mm between the glass cover and the absorber plate. The absorptivity of the glass cover was determined using a spectrophotometer, which measured the amount of radiation absorbed by the glass at different wavelengths [1, 4]. The glass cover has an absorption of 0.06, transmission of 0.86 and reflection of 0.08. Absorber and bottom plates are made of a 1 mm thick galvanized iron (GI) sheet which is painted black to enhance absorptivity. It has an absorptivity of 0.88, a transmittance of 0.08 and a reflectivity of 0.04. Wire ribs are tack welded at three points on the absorber plate as shown in Fig. 2. As the area occupied is very less it will not alter the thermal resistance and does not affect the results. Also, a commercially available high-temperature adhesive was used which is designed specifically for the use of solar thermal collectors. The adhesive has a thermal conductivity of 0.2 $W/(m^2K)$ and a thermal resistance of 0.001 K/W.
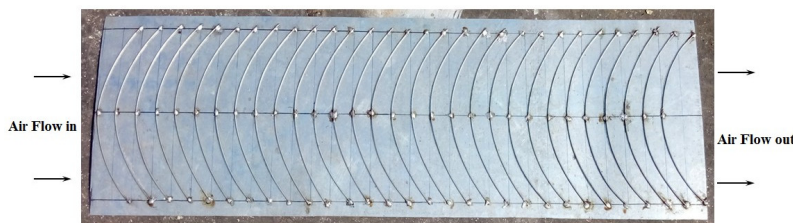

Figure 2: Photographic view of an arc-shape wire roughened absorber plate with apex upstream flow.

The photographic and schematic view of arc shape wire roughened absorber plate with apex upstream flow is shown in Figs. 2 and 3, respectively. Digital thermal temperature indicators which give temperature in °C were used to measure the air temperatures. They were installed at the inlet and outlet of the test section in both SAH ducts. Thermocouples (fifteen) were used to measure the absorber plate temperatures at different locations. Two micromanometers (one for smooth SAH and one for roughened SAH) (Flowtech) with an accuracy of ±0.01 mm of water column were used to measure pressure drop along the SAH test (ΔP_D) sections. A digital pyra-

nometer (Virtual Hydromet) with accuracy of $\pm 0.5\%$ was used for measuring the intensity of solar radiation on a horizontal surface.
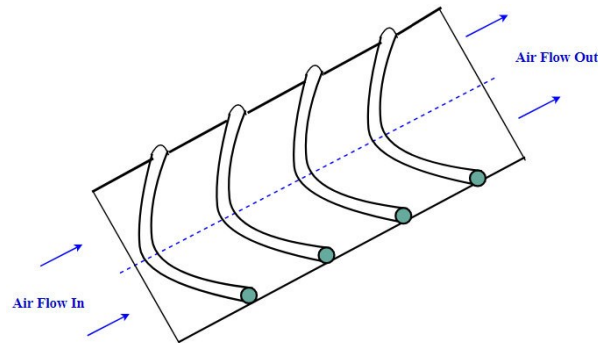

Figure 3: Absorber plate with roughness elements geometry.

2.1   Experimental procedure and data collection

Experimental runs were carried out outdoors under bright sunlight conditions between the months of March to May 2017 between 10.00 am and 4.00 pm on clear sky days. The readings were noted down when the system attained a steady state for at least 30 min. Figure 4 shows the variations of solar intensity versus local time (hrs) for some selected days on which
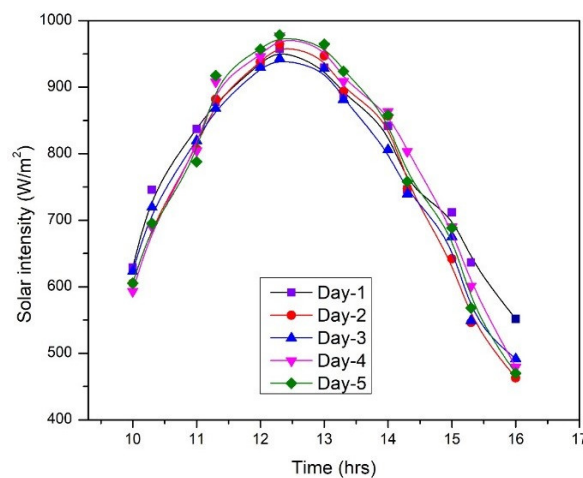

Figure 4: Variation of solar intensity versus local time for five different days.

the study was conducted. It can be seen, from Fig. 4 that solar intensity increases up to 1.00 pm and after that it starts decreasing.

2.2 Data reduction

The mass flow rate of air is calculated using equation [30, 31]:

$$\dot{m} = C_d A_o \sqrt{\frac{2\rho\Delta P_o}{1 - \beta_R^4}}\,, \tag{1}$$

where C_d is the coefficient of discharge evaluated by calibration which amounts to 0.61, whereas β_R is the ratio of orifice diameter (D_2) to air (fluid) flow pipe internal diameter (D_1) and equals 0.60. Parameter ρ stands for the air density and A_o represents the area of an orifice plate.

The pressure drop across the orifice meter (ΔP_0) was been calculated using the U-tube manometer fluid difference head (column) reading (Δh), having a 300 mm scale, with water as manometric fluid [29–31]:

$$\Delta P_o = \rho_u g \Delta h\,, \tag{2}$$

where ρ_u is the density of water (manometer fluid) and g is gravitational acceleration.

Useful heat energy gain by air was computed from [33, 34]

$$Q_u = \dot{m} C_{pa} \left(T_{fo} - T_{fi}\right), \tag{3}$$

Heat transfer coefficient for the test section ducts was computed using the expression [30, 31]

$$h = \frac{Q_u}{A_c(T_{pm} - T_{fm})}\,, \tag{4}$$

where A_c is the surface area of the absorber plate, and T_{pm} is the mean absorber plate temperature, which is the average of all temperatures measured by thermocouples located over the absorber plate (at 15 measurement points), and is calculated from

$$T_{pm} = \frac{1}{15} \sum_{i=1}^{15} T_i\,. \tag{5}$$

Temperature T_{fm} is an arithmetic mean of the entry (inlet) and exit temperature of the air flowing through the SAH duct and is expressed as [30,31]

$$T_{fm} = \frac{T_{fi} + T_{fo}}{2}\,. \tag{6}$$

Figure 5 shows the locations of thermocouples in the inlet (entry) and outlet (exit) sections, and on the absorber plate.
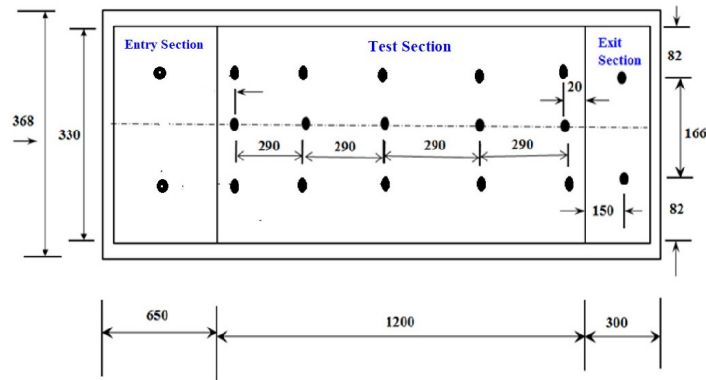

Figure 5: Locations of digital thermocouples in the entry and exit sections and on the absorber plate (all dimensions in mm).

The Nusselt number is given by [30, 31]

$$\text{Nu} = \frac{hD_h}{K_a} \,, \tag{7}$$

where K_a is the thermal conductivity of air, and D_h is the hydraulic diameter of the duct which can be calculated from

$$D_h = \frac{2WH}{W + H} \,. \tag{8}$$

The Reynolds number is evaluated by [30, 31]

$$\text{Re} = \frac{GD_h}{\mu} \,, \tag{9}$$

where μ is the absolute air viscosity and G is the mass velocity of air, which can be evaluated as

$$G = \frac{\dot{m}}{WH} \,. \tag{10}$$

To calculate the friction factor for SAHs, the following equation is used [30, 31, 33, 34]:

$$f = \frac{2\rho \Delta P_D D_h}{4L_f G^2} \,, \tag{11a}$$

where L_f is the distance between two pressure taps in the test section of the SAH duct. The pressure drop across the SAH test section (ΔP_D)

is calculated by using the micromanometer fluid difference head reading (Δh_1) which have the least count of 0.01 mm of water column:

$$\Delta P_D = \rho_m g \Delta h_1 \,. \tag{11b}$$

2.3 Thermal and thermo-hydraulic performance criterion

The thermal efficiency of a SAH can be determined using the equation [4]

$$\eta_{th} = \frac{Q_u}{I A_c} \,. \tag{12a}$$

The evaluation of the thermo-hydraulic performance criterion included both, the thermal and hydraulic performance of a SAH, as introduced by Webb and Eckert [7] and Lewis [6], and follows the equation:

$$\eta_{\text{THPP}} = \frac{\dfrac{\mathrm{Nu}_r}{\mathrm{Nu}_s}}{\left(\dfrac{f_r}{f_s}\right)^{1/3}} \,, \tag{12b}$$

where Nu_r , Nu_s and f_r , f_s are the Nusselt number and the friction factor for a roughened and smooth duct solar heater, respectively.

2.4 Thermo-hydraulic (effective) efficiency of solar air heater

The effective efficiency of the solar air heater was determined by considering pressure drop and the power needed to force the airflow across the SAH duct, in addition to thermal energy gain (Q_u). Hence, the thermo-hydraulic efficiency or effective efficiency takes both, i.e. pumping power and thermal energy gain, and is given by equation [35]

$$\eta_{\text{eff}} = \frac{Q_u - \dfrac{\dot{W}_p}{C_f}}{I A_c} \,, \tag{13}$$

where C_f is conversion factor and $\dot{W}_p$ is a pump work, which is defined as

$$\dot{W}_p = \frac{\dot{m} \Delta P_D}{\rho} \,. \tag{14}$$

2.5 Thermo-hydraulic improvement parameter

Thermo-hydraulic improvement parameter (THIP) which is applied as an optimization parameter in the present paper, can be evaluated as

$$\eta_{\text{THIP}} = \frac{\text{NNIF}}{\text{FFIF}}\,, \tag{15}$$

where NNIF is the Nusselt number improvement factor which is calculated (in percentage) by

$$\text{NNIF} = \frac{\text{Nu}_r - \text{Nu}_s}{\text{Nu}_s} \times 100 \tag{16}$$

and FFIF is the friction factor improvement factor which is expressed (in percentage) by

$$\text{FFIF} = \frac{f_r - f_s}{f_s} \times 100. \tag{17}$$

It can be seen from Eq. (15) that when NNIF is higher than FFIF the THIP becomes greater than 1 ($\eta_{\text{THIP}} > 1$), which is desirable for the use of any type of enhancement technique in the SAHs and also in other thermal systems.

2.6 Uncertainty analysis

An error analysis was done as per the methodology suggested by Kline and McClintock [26]. For the investigated roughened absorber solar air heaters, the maximum uncertainty values for dimensionless numbers are obtained as:

- thermal efficiency: $\pm 5.61\%$,

- Reynolds number: $\pm 4.87\%$,

- friction factor: $\pm 5.14\%$,

- thermo-hydraulic efficiency: $\pm 8.47\%$.

3 Experimental design and plan for optimization

3.1 Taguchi method

The Taguchi method is well-known method that has been used for the design of experiments (DOE) and as an optimization tool in different industries and numerous areas of engineering *via* experiments. It analyzes and evaluates all different design factors/parameters which are used in the

experiments and determines the best choices of factors/parameters that deliver us target optimum performance values by selecting desired control factors with the minimal number of experiment trails/runs.

The Taguchi method uses standard tables of experiments called orthogonal arrays (OA) which are represented by [24, 25]

$$\text{OA} = L_N A^n, \tag{18}$$

where L_N is the number of experimental/test runs, A denotes levels of the factors/variables and n is the number of factors.

For studying a large number of parameters with a lesser number of experimental trials (runs), the OA was adopted, and after that, the effect of main and interacting experimental parameters was converted into the signal-to-noise ratio (SN-R).

In the Taguchi method, firstly one has to choose and select the desired objective performance as the target function to which we have to optimized. After selecting the objective function, the control factors which are to be varied, are chosen. Then, the affecting factors are assigned with their levels according to experimentation, and these assigned control factors and their levels are numerically tested by the signal-to-noise ratio (SN-R) analysis.

3.2   Plan for optimization

In the present analysis, the number of test runs (N) was considered as 18. Furthermore, Reynolds number, relative roughness pitch and angle of attack were considered as factors (n) with their levels (A), 6, 3, and 3, respectively. Hence, we obtained an orthogonal array of $L_{18} = 6^1 \times 3^2$.

The present study accommodates the mixed L_{18} design array including three control factors: Reynolds number (Re), relative roughness pitch (P/e) and angle of attack (α) varying with levels 6, 3, and 3, respectively. The same is tabulated in Table 2.

Tables 3 and 4 tabulates 18 experimental runs based on the orthogonal array (OA) and a signal-to-noise ratio (SN-R) respectively, which was used to determine the sensitivity of the parameters on the physical behavior. It also presents the results obtained from the experimental runs which were converted into signal-to-noise ratio (SN-R).

The Taguchi technique defines an optimum condition as a case where least variation of a system performance is observed by noise factor or best SN-R represents optimum system configuration. Quality characteristics using SN-R are classified in two cases: higher-is-better (HB) and the lower-

Table 2: Control factors ($L_{18} = 6^1 \times 3^2$) used in the experiments with their values and levels.

Control factors		Level					
		I	II	III	IV	V	VI
A	Reynolds number (Re)	2983	4717	7459	9435	11556	13955
B	Relative roughness pitch (P/e)	8	10	15	–	–	–
C	Angle of attack (α), deg	45	60	75	–	–	–

Table 3: Experimental plan and results of OA ($L_{18} = 6^1 \times 3^2$) for control factors and output responses.

Exp. run number	Control factors			Results		
	A	B	C	Nusselt number	Friction factor	Thermo-hydraulic improvement parameter
	Reynolds number (Re)	Relative roughness pitch (P/e)	Angle of attack (α)	Nu	f_r	(η_{THIP})
1	2983	8	45	17.7	0.0202	54.98851
2	2983	10	60	19	0.0200	70.35294
3	2983	15	75	14.15	0.0176	24.88525
4	4717	8	45	29.95	0.0188	87.40027
5	4717	10	60	31.5	0.0184	103.04380
6	4717	15	75	22.94	0.01635	54.20538
7	7459	8	45	50.96	0.0174	118.40960
8	7459	10	60	53.2	0.0172	131.60490
9	7459	15	75	40.94	0.0152	100.10300
10	9435	8	45	67.04	0.0168	127.93730
11	9435	10	60	72.12	0.0166	149.21850
12	9435	15	75	54.45	0.01465	114.14260
13	11556	8	45	84.93	0.0163	147.97850
14	11556	10	60	91.59	0.0161	171.76220
15	11556	15	75	69.14	0.014	141.95300
16	13955	8	45	105.9	0.0158	153.11290
17	13955	10	60	112.5	0.0156	173.05830
18	13955	15	75	85.4	0.0136	144.2752

is-better (LB). The characteristic equations for these two cases are, respectively:

for higher-is-better:

$$\mathrm{SN-R} = -10\log\left(\frac{1}{N}\sum\frac{1}{y^2}\right) \tag{19}$$

and for lower-is-better:

$$\mathrm{SN-R} = -10\log\left(\frac{1}{N}\sum y^2\right), \tag{20}$$

where N is the number of experimental runs, and y^2 is the observed experimental data.

Table 4 represents the experimental plan and its signal-to-noise ratio. In the present analysis, the Nusselt number and thermo-hydraulic improvement parameters are considered as higher-is-better criterion, whereas the friction factor for the roughened surface (f_r) is considered as a lower-is-better criterion.

Table 4: Experimental design (L_{18}) with its SN-R values.

Exp. run number	Results					
	Nusselt number	Signal-to-noise ratio	Friction factor	Signal-to-noise ratio	Thermo-hydraulic improvement parameter	Signal-to-noise ratio
1	17.70	24.95947	0.0202	33.89297	54.98851	34.80544
2	19.00	25.57507	0.0200	33.97940	70.35294	36.94565
3	14.15	23.01513	0.0176	35.08975	24.88525	27.91884
4	29.95	29.52794	0.0188	34.51684	87.40027	38.83026
5	31.50	29.96621	0.0184	34.70364	103.04380	40.26044
6	22.94	27.21187	0.01635	35.72964	54.20538	34.68085
7	50.96	34.14459	0.0174	35.18902	118.40960	41.46774
8	53.20	34.51823	0.0172	35.28943	131.60490	42.38544
9	40.94	32.24296	0.0152	36.36313	100.10300	40.00895
10	67.04	36.52668	0.0168	35.49381	127.93730	42.13995
11	72.12	37.16111	0.0166	35.59784	149.21850	43.47646
12	54.45	34.71996	0.01465	36.68325	114.14260	41.14896

Table 1. *Continued from previous page.*

Exp. run number	Results					
	Nusselt number	Signal-to-noise ratio	Friction factor	Signal-to-noise ratio	Thermo-hydraulic improvement parameter	Signal-to-noise ratio
13	84.93	38.58122	0.0163	35.75625	147.9785	43.40397
14	91.59	39.23696	0.0161	35.86348	171.76220	44.69855
15	69.14	36.79459	0.014	37.07744	141.9530	43.04289
16	105.90	40.49792	0.0158	36.02686	153.1129	43.70023
17	112.50	41.02305	0.0156	36.13751	173.0583	44.76385
18	85.40	38.62916	0.0136	37.32922	144.2752	43.18383

The application of the Taguchi method and its procedure which is used for the present investigation is given by the flow chart shown in Fig. 6.
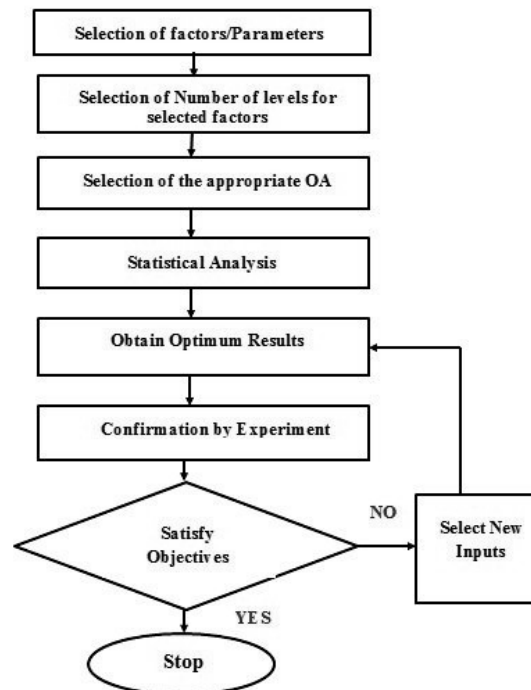
Figure 6: Flow chart of the Taguchi method for optimal design.

4   Result and discussion

4.1   Thermal efficiency

By using the present apex-upstream roughened SAH the maximum thermal efficiency of 65.2% has been observed, corresponding to $e/D_h = 0.0454$, $P/e = 10$, $\alpha = 60$ deg and for the highest Reynolds number considered in the present analysis, i.e. Re = 13955, while for the smooth plate SAH the maximum thermal efficiency obtained for the highest Reynolds number was 41.4%.

4.2   Comparison of Nusselt numbers in SAH duct

Figure 7 shows the comparison of experimental values of the Nusselt number for roughened duct and smooth plate SAH as a function of Reynolds number for different values of relative roughness pitch. The other fixed parameters, $\alpha = 60$ deg and $e/D_h = 0.0454$, are shown in the figure. It is observed that Nu for both SAHs increases with increasing Re values, however, the Nu values for roughened SAH are larger compared to the smooth plate SAH. Furthermore, the maximum value of Nu was attained at the relative roughness pitch (P/e) of 10.
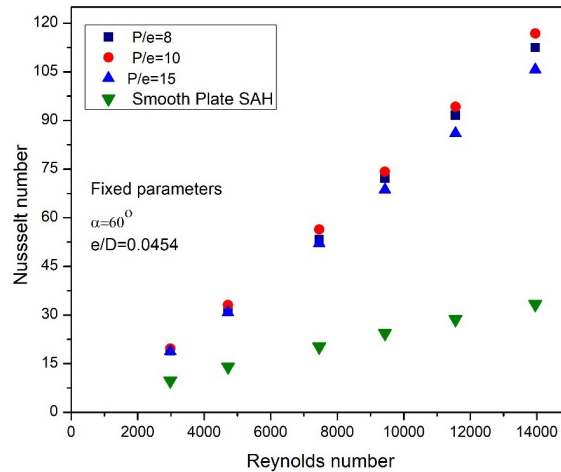

Figure 7: Effect of relative roughness pitch (P/e) on Nusselt number as a function of Reynolds number for apex-upstream roughened SAH and smooth plate SAH.

Figure 8 shows the comparison of the Nusselt number change with the Reynolds number between the smooth plate SAH and the apex-upstream

roughened SAH at various angles of attack. It can be observed that Nu attains maximum value for roughened SAH of $\alpha = 60$ deg.
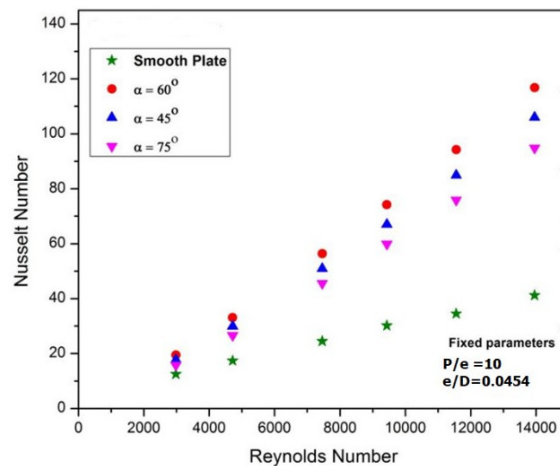

Figure 8: Effect of angle of attack (α) on Nusselt number as a function Reynolds number for apex-upstream roughened SAH and smooth plate SAH.

4.3   Comparison of SAH duct pressure drop

Figures 9 and 10 show the comparison of experimental values of pressure drop in the roughened duct and the smooth plate SAH for different Reynolds number values. Figure 9 shows the comparison of the pressure drop variation (ΔP_D) for the roughened duct with different values of the relative roughness pitch (P/e) and fixed values of $\alpha = 60$ deg and $e/D_h = 0.0454$ with that for the smooth plane SAH as a function of Reynolds number. It can be observed from the figure that ΔP_D increases for both SAH ducts with an increase in the values of Re, and ΔP_D values for smooth duct are lower compared to those for roughened SAH for all values of Re.

Figure 10 shows the comparison of pressure drop (ΔP_D) between the apex-upstream roughened SAH with different values of α, and for the smooth plate SAH as function of Re. It can be seen from the figure that pressure drop for both SAHs increases with increasing Re, however, the values of ΔP_D for roughened SAH are larger as compared to the smooth plate SAH. Furthermore, it is observed that the maximum value of ΔP_D corresponds to $\alpha = 60$ deg for roughened SAH.
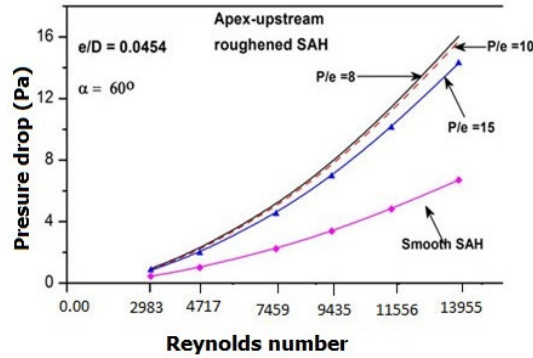
Figure 9: Effect of relative roughness pitch (P/e) on pressure drop as a function of Reynolds number for apex-upstream roughened SAH and smooth SAH.
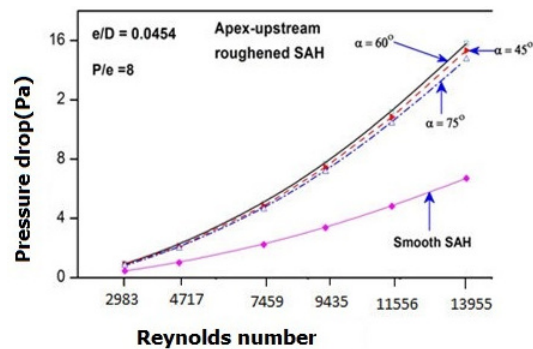

Figure 10: Effect of angle of attack (α) on the pressure drop as a function of Reynolds number for apex-upstream roughened and smooth SAHs.

4.4   Analysis

Figures 11–13 represent the mean effect plots for Nusselt number, friction factor, and thermo-hydraulic improvement parameter, respectively. Their performance values and results obtained are presented in Tables 5–7.

Figure 11 shows the effect of three control factors: A, B, and C on Nu and it can be observed from the figure that there is a continuous increase in Nusselt number as factor A (Re) increases from level 1 to 6. This is because by increasing the Re, turbulent intensity increases in the fluid flow inside the duct. Thus, higher values of mass flow rate result in higher rates of heat transfer coefficient h, and hence in higher values of Nu. Furthermore, it can be seen from Table 5) and Fig. 11, that Nu increases with an increase in
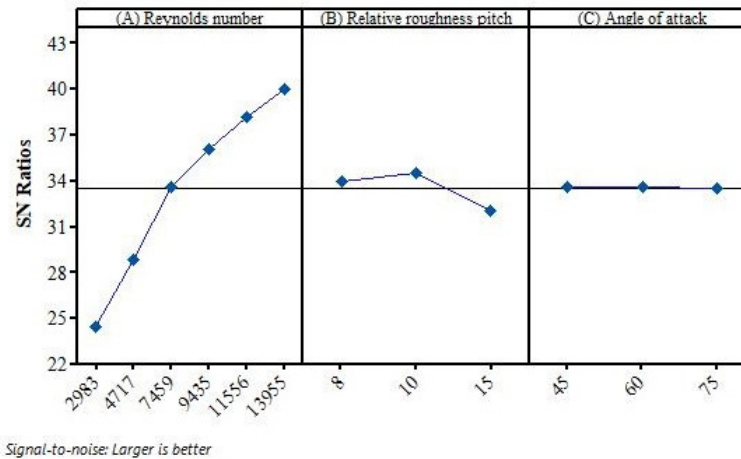
Figure 11: Variation of Nusselt number with change in the design parameters of A, B, and C.

the factor B (P/e) from 1st level to 2nd level and after that, it decreases down to 3rd level with further P/e increase. In the present analysis, the maximum value of Nu is observed at $P/e = 10$. This is due to the reason that number of reattachment points decreases (which in turn reduces the heat transfer rate) with an increase in the value of P/e. It is reported by the researchers that maximum heat transfer occurs at the attachment points between two roughness ribs (also called inter-rib space) and the reattachment of the flow between two roughness ribs does not occur for the higher values of pitch. Reattachment of flow occurs for $P/e > 8$ while the optimum value for maximum heat transfer varies in the P/e range of 8–12, which again depends on the type of rib roughness and its geometries used on the absorber plate. For factor C (α), the Nusselt number slightly increases from 1st level to 2nd level with an increase in α from 45 to 60 deg and after that, it decreases. The Nu has its lowest value for $\alpha = 75$ deg in the present analysis while the maximum value of Nu was obtained for $\alpha = 60$ deg. Angling roughness ribs creates span-wise counter-rotating secondary flow along the length of the absorber plate in the test section, which enhances the heat transfer coefficient significantly. Furthermore, due to alignment of ribs at an angle with respect to flow on the absorber plate the vortices creates on the upstream and downstream sides of the ribs. These vortices move along the flow at the absorber plate surfaces and merge with the (main) core flow and thus helps in increasing the heat transfer rate. The generation

of secondary flows and vortices occurs maximum for the alignment of ribs at an angle of $\alpha = 60$ deg for the present roughness geometry.

In Table 5, Delta is the difference between the highest and lowest average response values for each factor. After calculation of Delta values, the factor which have highest Delta value has been assign as Rank 1, the factor which have second highest Delta value has been assign as Rank 2 and so on.

Table 5: Response table for signal-to-noise ratios (SN-R) for Nusselt number (Nu).

Level	A (Re)	B (P/e)	C (α)
1	24.52	34.04	33.60
2	28.90	34.58	33.62
3	33.64	32.10	33.50
4	36.14	–	–
5	38.20	–	–
6	40.05	–	–
Delta	15.53	2.48	0.12
Rank	1	2.00	3.00

Figure 12 shows the effect of three control factors on the friction factor f_r. Furthermore, from Fig. 12 and Table 6 it can be seen that f_r attains its
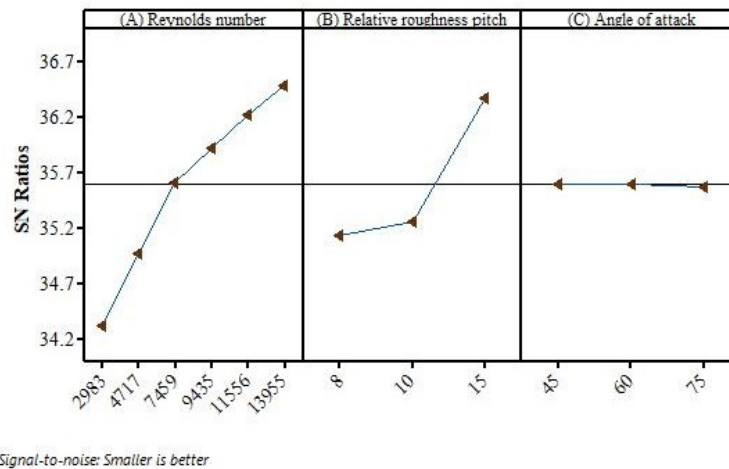

Figure 12: The effects of design parameters of A, B, and C on the friction factor.

minimum value corresponding to control factors A (Re) = 2983, B (P/e) = 8 and C (α) = 45 deg. In the present analysis, the friction factor has its minimum for $P/e = 8$ and $\alpha = 45$ deg because at these values of roughness parameters least turbulence is developed in the fluid flow and due to this less pressure drop in the SAH duct takes place, which results in the lowest values of friction factor.

Table 6: Response table for signal-to-noise ratios (SN-R) for friction factor (f_r).

Level	A (Re)	B (P/e)	C (α)
1	34.32	35.15	35.60
2	34.98	35.26	35.62
3	35.61	36.38	35.58
4	35.92	–	–
5	36.23	–	–
6	36.50	–	–
Delta	2.18	1.23	0.02
Rank	1	2	3

Figure 13 represents the mean effects of control factors on THIP. As demonstrated in the figure, an increasing trend can be observed for THIP for all values of control factor A (Re). It can also be seen that growth in THIP
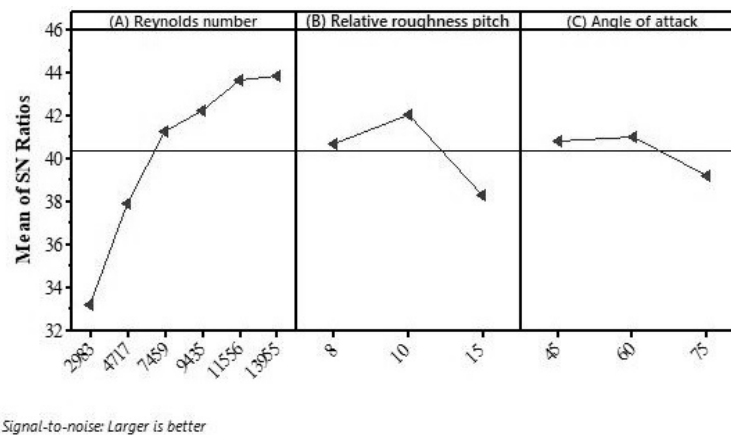

Figure 13: The effects of design parameters of A, B and C on the thermo-hydraulic improvement parameter (THIP).

is steeper up to the 3rd level of Re = 7459 and afterward, with further increase in Re the THIP curve increment rate is relatively lower. This is due to the reason that when the value of Re increases, there is an increment in the pressure drop and pumping power in the SAH duct, as THPP is the ratio of the Nusselt number improvement factor to the friction factor improvement factor (Eq. (15)) and at a higher range of Re the enhancement in friction factor and pressure drop is more dominant (or relatively more) over the enhancement in the heat transfer coefficient and Nu. Furthermore, from Fig. 13 and Table 7, it can be concluded that the highest THIP is observed for Re = 13955, $P/e = 10$ and $\alpha = 60$ deg.

Table 7: Response table for signal-to-noise ratios (SN-R) for thermo-hydraulic improvement parameter (THIP).

Level	A (Re)	B (P/e)	C (α)
1	33.22	40.72	40.82
2	37.92	42.09	41.07
3	41.29	38.33	39.25
4	42.26	–	–
5	43.72	–	–
6	43.88	–	–
Delta	10.66	3.76	1.81
Rank	1	2	3

4.5 Contribution ratio

Figure 14 represents the detailed representation of the contribution ratio percentage of each control factor to the Nusselt number, friction factor, and thermo-hydraulic improvement parameters. It can be seen from the figure that the parameter A (Re) contributes to 94.09% for Nu, 66.17% for (f_r) and 85.85% for THIP, respectively, of the total effect. This reveals that Nu, f_r, and THIP are majorly affected by parameter A. As it can be seen, the parameter B (P/e) contribution ratio is 4.74% for Nu, and parameter C (α) contribution ratio for Nu is 1.18%. The contribution ratios of factors B and C for friction factor are 33.65%, and 0.18%, respectively. Hence, it can be concluded, that Reynolds number (A) is the most effective parameter that affects the performance of roughened SAH, i.e. the Nusselt number, friction

factor and thermo-hydraulic improvement parameter, more than P/e and α. The contribution ratios of each control factor on every performance parameter are tabulated in Table 8. Thus, the optimum level of control factors for Nu is $A_6B_2C_2$, for f_r is $A_1B_1C_3$ and for THIP is $A_6B_2C_2$, which are also shown in Fig. 15.
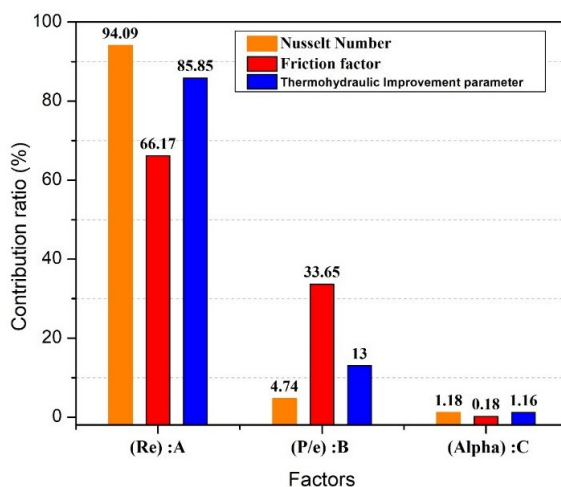

Figure 14: The contribution ratio of each parameter to Nusselt number, friction factor and thermo-hydraulic improvement parameter.
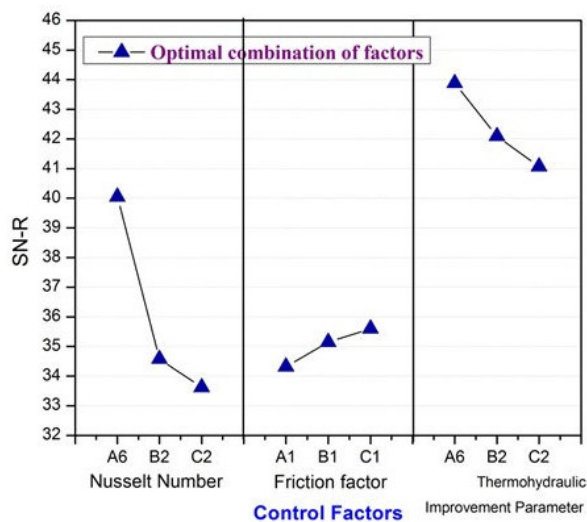

Figure 15: Optimal combination of control factors for Nu, f_r and THIP.

Table 8: Optimum performance conditions and the contribution ratios of each control factors on the different performances.

	Parameter		
	A	B	C
	Reynolds number (Re)	Relative roughness pitch (P/e)	Angle of attack (α)
Nusselt number (Nu)			
Optimum level	Level – VI	Level – II	Level – II
Optimum value	13955	10	60 deg
Contribution ratio	94.09%	4.74%	1.18%
Friction factor (f)			
Optimum level	Level – I	Level – I	Level – I
Optimum value	2983	8	45 deg
Contribution ratio	66.17%	33.65%	0.18%
Thermo-hydraulic improvement parameter (THIP)			
Optimum level	Level – VI	Level – II	Level – II
Optimum value	13955	10	60 deg
Contribution ratio	85.85%	13%	1.16%

5   Experiments for confirmation

In the Taguchi design of the experimental method, a confirmation experiment is done to validate the results. This is performed by consideration of a new set of control factors which is further done by setting $A_6B_2C_2$, $A_1B_1C_3$, and $A_6B_2C_2$ to predict the Nusselt number, friction factor, and thermo-hydraulic improvement parameter, while Table 9 takes into account the results of confirmation tests carried out with optimum design parameters.

The estimated value of signal-to-noise for Nu, f_r, and THIP were calculated by taking a summation of an average performance by considering the contribution of each parameter at an optimum level using the following equations [16, 17]:

$$\eta_{\mathrm{Nu}} = \overline{T_{\mathrm{Nu}}} + \left(A_6 - \overline{T_{\mathrm{Nu}}}\right) + \left(B_2 - \overline{T_{\mathrm{Nu}}}\right) + \left(C_2 - \overline{T_{\mathrm{Nu}}}\right), \qquad (21)$$

$$\eta_{f_r} = \overline{T_f} + \left(A_1 - \overline{T_{f_r}}\right) + \left(B_1 - \overline{T_{f_r}}\right) + \left(C_3 - \overline{T_{f_r}}\right) \qquad (22)$$

and

$$\eta_{\text{THIP}} = \overline{T_{Nu}} + \left(A_6 - \overline{T_{\text{THIP}}} \right) + \left(B_2 - \overline{T_{\text{THIP}}} \right) + \left(C_2 - \overline{T_{\text{THIP}}} \right), \quad (23)$$

where $\overline{T}$ represents the average experimental temperature and A_6, B_2, C_2 is the mean response for factors at designated levels for Nu.

A comparison of values of Nu, f_r, and THIP obtained from both experiments and the prediction are presented in Table 9. As can be seen from the comparison of initial parameters and optimum parameters obtained from the Taguchi method, shown in the table, an improvement in the SN ratio for Nu is 16.16 dB with an error of 15.90%. The obtained improvement in the SN ratio for f_r is 4.2 dB with an error of 6.56% while the achieved improvement in the SN ratio for THIP is 11.48 dB with an error of 12.74%. This indicates that the experimental results are very close to the predicted results. The results obtained from confirmation experiments proved the validity of the Taguchi approach used in the optimization of the design parameters.

Table 9: Results of the confirmation experiment

Parameters		Initial parameters	Optimum control parameters		
			Prediction	Experimental	Improvement of signal-to-noise ratio, dB
Nusselt number (Nu)	Level	$A_1B_1C_1$	$A_6B_2C_2$	$A_6B_2C_2$	–
	SN-R, dB	24.95	34.57	41.11	16.16
Friction factor (f)	Level	$A_1B_1C_1$	$A_1B_1C_3$	$A_1B_1C_3$	–
	SN-R, dB	33.89	35.59	38.09	4.2
Thermo-hydraulic improvement parameter (THIP)	Level	$A_1B_1C_1$	$A_6B_2C_2$	$A_6B_2C_2$	–
	SN-R, dB	34.80	40.38	46.28	11.48

6   Conclusions

The present study applies the Taguchi design of experimental methods, to find the configuration of a set of roughness and flow parameters to maximize the Nusselt number and the thermo-hydraulic improvement parameter, and minimize the losses due to friction for a roughened solar air heater (SAH). Further, the Reynolds number, relative roughness pitch, and angle of attack

were taken as control factors for the present study. Based on the results of the investigation, the following conclusions are drawn.

1. The Nusselt number, friction factor and thermo-hydraulic improvement parameter are very much influenced by the control factors *viz.* the Reynolds number, relative roughness pitch, and angle of attack.

2. The contribution ratio of the control factors: Reynolds number (A), relative roughness pitch (B), and angle of attack (C), on the Nusselt number (Nu) is 94.09%, 4.74%, and 1.18%, respectively. For the friction factor (f_r) it is 66.17%, 33.65%, and 0.18%, and for the thermo-hydraulic improvement parameter (THIP) it is 85.85%, 13.00%, and 1.16%, respectively.

3. An optimal value of the parameters for maximum Nu is $A_6B_2C_2$, i.e. Reynolds number of 13955, relative roughness pitch of 10, and angle of attack of 60 deg. The optimal condition for minimum friction factor is $A_1B_1C_3$, i.e. Reynolds number of 2983, relative roughness pitch of 8, and an angle of attack of 45 deg. For maximum thermo-hydraulic improvement parameter the combination of optimal design parameters is $A_6B_2C_2$, i.e. Reynolds number of 13955, relative roughness pitch of 10, and angle of attack of 60 deg.

4. The experimental confirmation shows a 16.16 dB improvement in the signal-to-noise ratio (SN-R) for the Nusselt number. For the friction factor and thermo-hydraulic improvement parameter, it shows 4.2 dB and 11.48 dB improvements in SN-R values, respectively.

5. The Taguchi method is most effective when dealing with a small number of factors and parameters that can be controlled. In the present analysis, there are only 3 control factors considered. There are also many factors that affect the performance of the solar air heater such as type of absorber plate material, flow rate of air, wind velocity, angle, and orientation of the SAH, etc.

It may be challenging to design an experiment that includes all relevant factors and interactions. In the future, researchers can consider other control factors for their analysis.

The results of this study show that that using for the present roughened solar air heater an optimized configuration of roughness and flow parameters, which are obtained by applying the Taguchi method there is no need to run the experimental set-up all 54 times.

References

[1] Khan B.H.: *Non-Conventional Energy Resources* (2nd Edn.). Tata McGraw Hill, New Delhi 2012.

[2] Sahu M.K., Prasad R.K.: *A review of the thermal and hydrodynamic performance of solar air heater with roughened absorber plates.* J. Enhanc. Heat Transf. **23**(2016), 47–89.

[3] Sahu M.K., Sharma M., Matheswaran M.M., Maitra K.: *On the use of various configurations of fins to enhance the performance in rectangular duct of solar air heaters – A review.* J. Sol. Energy Eng. **141**(2019), 3, 030802.

[4] Duffie J.A., Beckman W.A.: *Solar Engineering of Thermal Processes* (2nd Edn.). Wiley, New York 1991.

[5] Sahu M.K., Priyam A., Mishra S., Bishnoi P.: *A detailed review on research, technology, configurations and application of wire ribs as artificial roughness in rectangular solar air heater duct.* Proc. Inst. Mech. Eng. E J. Process Mech. Eng. **235**(2021), 4, 1211–1234.

[6] Lewis M.J.: *Optimizing the thermohydraulic performance of rough surfaces.* Int. J. Heat Mass Tran. **18**(1975), 1243–1248.

[7] Webb R.L., Eckert E.R.G.: *Application of rough surface to heat exchanger design.* Int. J. Heat Mass Tran. **15**(1972), 1647–1658.

[8] Varun, Sharma N., Bhat I.K., Grover D.: *Optimization of a smooth flat plate solar air heater using stochastic iterative perturbation technique.* Sol. Energy **85**(2011), 2331–2337.

[9] Rao R.V., Waghmare G.: *Optimization of thermal performance of a smooth flat-plate solar air heater using teaching-learning-based optimization algorithm.* Cogent. Eng. **2**(2015), 3–28.

[10] Siddhartha, Sharma N., Varun: *A particle swarm optimization algorithm for optimization of thermal performance of a smooth flat plate solar air heater.* Energy **38**(2012), 406–413.

[11] Chamoli S.: *Preference selection index approach for optimization of V down perforated baffled roughened rectangular channel.* Energy **93**(2015), 1418–1425.

[12] Chauhan R., Singh T., Thakur N.S., Patnaik A.: *Optimization of parameters in solar thermal collector provided with impinging air jets based upon preference selection index method.* Renew. Energ. **99**(2016), 118–126.

[13] Bilen K., Yapici S., Celik C.: *A Taguchi approach for investigation of heat transfer from a surface equipped with rectangular blocks.* Energ. Convers. Manage. **42**(2001), 951–961.

[14] Varun, Patnaik A., Saini R.P., Singal S.K, Siddhartha: *Performance prediction of solar air heater having roughened duct provided with transverse and inclined ribs as artificial roughness.* Renew. Energ. **34**(2009), 2914–2922.

[15] Aghaie A.Z., Rahimi A.B., Akbarzadeh A.: *A general optimized geometry of angled ribs for enhancing the thermo-hydraulic behavior of a solar air heater channel – A Taguchi approach.* Renew. Energ. **83**(2015), 47–54.

[16] Chauhan R., Singh T., Kumar N., Patnaik A., Thakur N.S.: *Experimental investigation and optimization of impinging jet solar thermal collector by Taguchi method.* Appl. Therm. Eng. **116**(2017), 100–109.

[17] Chamoli S.: *A Taguchi approach for optimization of flow and geometrical parameters in a rectangular channel roughened with V down perforated baffles.* Case Stud. Therm. Eng. **5**(2015), 59–69.

[18] Hu J., Liu K., Ma L., Su X.: *Parameter optimization of solar air collectors with holes on baffle and analysis of flow and heat transfer characteristics.* Sol. Energy **174**(2018), 878–887.

[19] Turgut E., Cakmak G., Yildiz C.: *Optimization of the concentric heat exchanger with injector turbulators by Taguchi method.* Energ. Convers. Manage. **53**(2012), 268–275.

[20] Chamoli S., Yu P., Kumar A.: *Multi-response optimization of geometric and flow parameters in a heat exchanger tube with perforated disc inserts by Taguchi Grey relational analysis.* Appl. Therm. Eng. **103**(2016), 1339–1350.

[21] Kotcioglu I., Cansiz A., Khalaji M.N.: *Experimental investigation for optimization of design parameters in a rectangular duct with plate-fins heat exchanger by Taguchi method.* Appl. Therm. Eng. **50**(2013), 604–613.

[22] Chamoli S., Yu P., Yu S.: *Multi-objective shape optimization of a heat exchanger tube fitted with compound inserts.* Appl. Therm. Eng. **117**(2017), 708–724.

[23] Zeng M., Tang L.H., M. Lin M., Wang Q.W.: *Optimization of heat exchangers with vortex-generator fin by Taguchi method.* Appl. Therm. Eng. **30**(2010), 1775–1783.

[24] Taguchi G.: *Taguchi Techniques for Quality Engineering. Quality Resources.* McGraw-Hill, New York 1987.

[25] Ross P.J.: *Taguchi Techniques for Quality Engineering.* McGraw-Hill, New York, 1988.

[26] Kline S.J., McClintock F.P.: *Describing uncertainties in single sample experiments.* Mech. Eng. **75**(1953), 3–8.

[27] Taguchi G., Konishi S.: *Orthogonal Arrays and Linear Graphs: Tools for Quality Engineering.* American Supplier Institute, Dearborn 1987.

[28] Taguchi G., Jugulum R.: *The Mahalanobis Taguchi Strategy. A Pattern Technology System.* Wiley, New York 2002.

[29] Roy R.K.: *Design of Experiments Using the Taguchi Approach.* Wiley, Hoboken 2001.

[30] Sahu M.K, Matheswaran M.M., Bishnoi P.: *Experimental study of thermal performance and pressure drop on a solar air heater with different orientations of arc-shape rib roughness.* J. Therm. Anal. Calorim. **144**(2021), 1417–1434.

[31] Sahu M.K., Matheswaran M.M., Bishnoi P.: *Experimental investigation of augmented thermal and performance characteristics of solar air heater ducts due to varied orientations of roughness geometry on the absorber plate.* Arch. Thermodyn. **41**(2020), 3, 147–182.

[32] ASHRAE Standard 93-97. Method of testing to determine the thermal performance of solar collector. 1977.

[33] Sahu M.K., Prasad R.K.: *Second law optimization and parametric study of a solar air heater having artificially roughened absorber plate.* Arch. Thermodyn. **40**(2019), 2, 107–135.

[34] Sahu M.K., Prasad R.K.: *Thermohydraulic performance analysis of an arc shape wire roughened solar air heater.* Renew. Energ. **108**(2017), 598–614.

[35] Cortes A., Piacentini R.: *Improvement of efficiency of a bare solar collector by means of turbulence promoters.* Appl. Energ. **36**(1990), 253–261.